JACS
JOURNAL OF THE AMERICAN CHEMICAL SOCIETY
Communication
Cite This: J. Am. Chem. Soc. XXXX, XXX, XXX−XXX
pubs.acs.org/JACS

Ligand-Directed Reticular Synthesis of Catalytically Active Missing Zirconium-Based Metal−Organic Frameworks

Zhijie Chen,[†] Penghao Li,[†] Xingjie Wang,[†] Ken-ichi Otake,[†] Xuan Zhang,[†] Lee Robison,[†] Ahmet Atilgan,[†] Timur Islamoglu,[†] Morgan G. Hall,[‡] Gregory W. Peterson,[‡] J. Fraser Stoddart,[†,§,∥] and Omar K. Farha*[,†]

[†]Department of Chemistry and International Institute of Nanotechnology, Northwestern University, 2145 Sheridan Road, Evanston, Illinois 60208, United States

[‡]U.S. Army Combat Capabilities Development Command Chemical Biological Center, 8198 Blackhawk Road, Aberdeen Proving Ground, Maryland 21010, United States

[§]Institute for Molecular Design and Synthesis, Tianjin University, 92 Weijin Road, Tianjin 300072, China

[∥]School of Chemistry, University of New South Wales, Sydney, NSW 2052, Australia

Supporting Information

ABSTRACT: Zirconium-based metal−organic frameworks (Zr-MOFs) based on *edge-transitive* nets such as **fcu**, **spn**, **she**, **csq**, and **ftw** with diverse potential applications have been widely reported. Zr-MOFs based on the highly connected 6,12-connected **alb** net, however, remain absent on account of synthetic challenges. Herein we report the ligand-directed reticular syntheses and isoreticular expansion of a series of Zr-MOFs with the edge-transitive **alb** net from 12-connected hexagonal-prismatic Zr_6 nodes and 6-connected trigonal-prismatic linkers, i.e., microporous NU-1600, mesoporous NU-1601, and mesoporous NU-1602. These Zr-MOFs exhibit remarkable activities toward the destruction of a nerve agent (soman) and a nerve agent simulant (DMNP).

Metal−organic frameworks (MOFs),[1−3] composed of inorganic nodes and organic linkers, are a class of porous crystalline materials with a wide range of applications, including but not limited to heterogeneous catalysis,[4−9] selective sensing,[10−12] water remediation,[13,14] and gas storage and separation.[15−19] Reticular chemistry[20−25] permits the rational top-down design and precise assembly of MOFs at the molecular level from the diverse choices of inorganic and organic building units. Consequently, MOFs have highly programmable structures with tunable pore sizes and apertures, high surface areas, and diverse functionality.[7,15−17,26−29]

Zirconium-based MOFs[28,30] (Zr-MOFs) represent a remarkable MOF subclass on account of the strong Zr−O coordination bond, and they have received considerable attention in the field since the first Zr-MOF—i.e., UiO-66 (where "UiO" denotes "University of Oslo") with Zr_6 inorganic building blocks and the 12-connected (12-c) **fcu** topology—was reported.[3] Tremendous efforts have been devoted to the development of Zr-MOFs based on *edge-transitive* nets—i.e., nets with one type of edge—because of the upsurge in reticular chemistry and versatile connectivity of polynuclear Zr clusters.[28] Many applications of these Zr-MOFs have been investigated, from heterogeneous catalysis[4,8] to water capture.[31,32] These edge-transitive networks include but are not limited to **spn** (e.g., MOF-808;[31] triangle and trigonal antiprism), **she** (e.g., PCN-224;[33] square and hexagon), **hxg** (e.g., **pbz**-MOF-1;[34] hexagon), **the** (e.g., NU-1200[35]/BUT-12;[36] triangle and cube), **csq** (e.g., PCN-222[37]/MOF-545[38] and NU-1000;[39] square and cube), **flu** (e.g., PCN-521;[22] tetrahedron and cube), **reo** (e.g., DUT-51;[40] cube); **ftw** (e.g., MOF-525[38] and MOF-1211;[41] square and cuboctahedron), **ith** (e.g., MOF-812;[31] tetrahedron and icosahedron), and **shp** (e.g., PCN-223;[42] square and hexagonal prism) (see Table S2 for a complete list). Nevertheless, an important class of Zr-MOFs based on a highly connected edge-transitive net, the 6,12-c **alb** net,[21,24,43] (trigonal prism and hexagonal prism; "**alb**" denotes "aluminum diboride"), has yet to be reported, most likely because of the lack of synthetic accessibility of the rigid trigonal-prismatic ligands and suitable assembly conditions. Higher connectivity in MOF structures permits an increased degree of controllability and designability. It is important to note that the synthesis of **alb**-MOFs based on rare-earth polynuclear clusters and indium trimers employing reticular chemistry has been reported recently by the Eddaoudi group.[24,43]

Herein we report the reticular synthesis of a Zr-MOF with the rare 6,12-c **alb** net, NU-1600, constructed from threefold-disordered Zr_6 nodes[42,44] and the peripherally extended triptycene (H_6PET-1) ligands[25,45] with a rigid trigonal-prismatic shape. Single-crystal X-ray diffraction (SCXRD) analysis revealed that the 6-c trigonal-prismatic PET-1 ligands and the 12-c Zr_6 nodes act as rare hexagonal-prismatic secondary building units (SBUs), leading to the assembly of 3-periodic NU-1600 with the **alb** net (Figure 1). NU-1600 is microporous, with an apparent Brunauer−Emmett−Teller (BET) surface area of 2085 $m^2\ g^{-1}$ and an experimental pore volume (PV) of 0.82 $cm^3\ g^{-1}$, as revealed by its N_2 adsorption isotherm at 77 K. The expanded mesoporous isoreticular structures—i.e., NU-1601 and NU-1602, with experimental PVs of up to 2.36 $cm^3\ g^{-1}$—can be readily synthesized (Figure S1) with extended ligands, namely, H_6PET-2 and H_6PET-3, respectively. On account of the Lewis acidic Zr sites, NU-1600 exhibits excellent catalytic

Received: June 10, 2019

DOI: 10.1021/jacs.9b06179
J. Am. Chem. Soc. XXXX, XXX, XXX−XXX

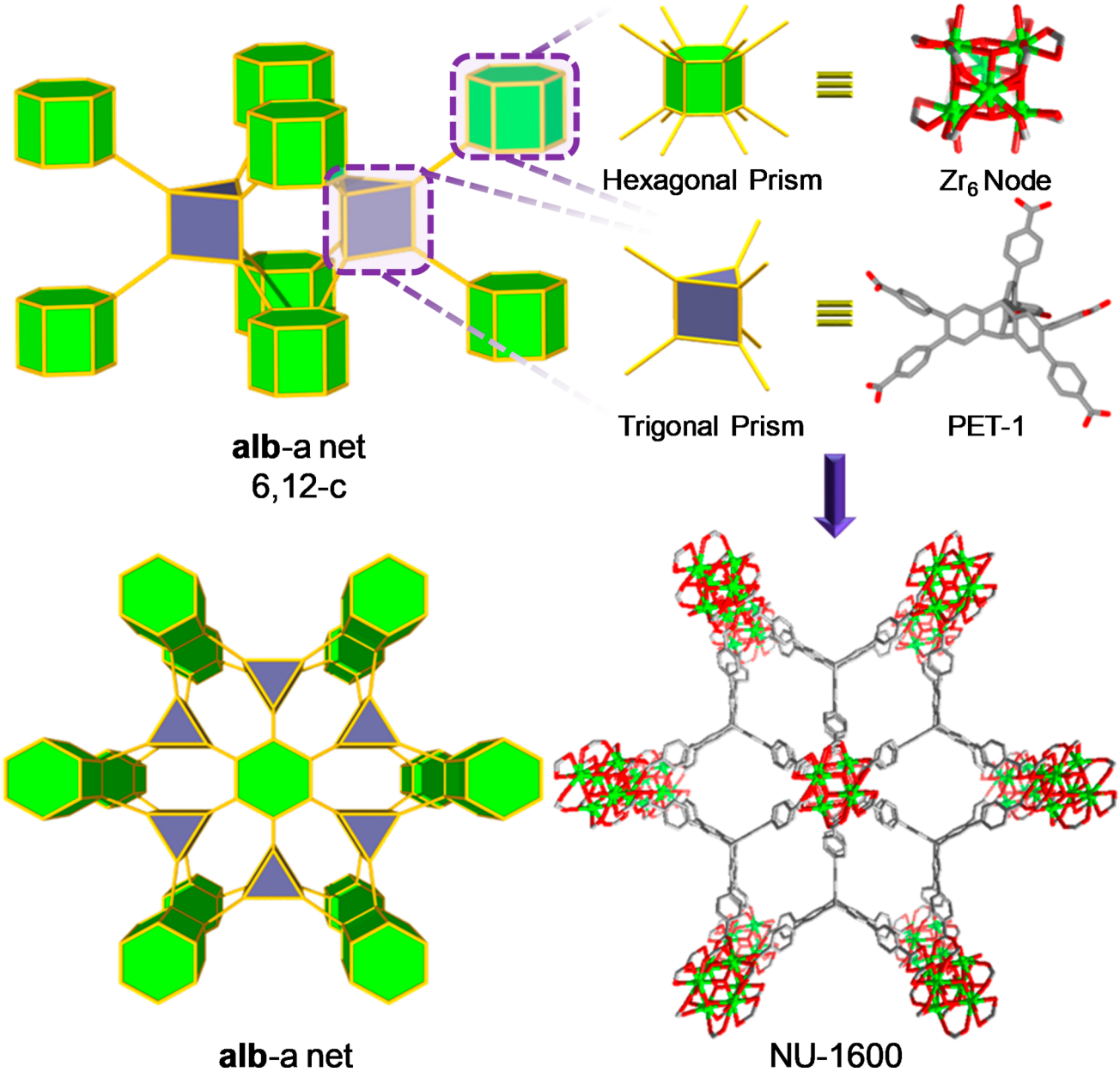

Figure 1. Top-down design and synthesis of a highly connected Zr-MOF with rigid trigonal-prismatic linkers, NU-1600, based on the 6,12-c edge-transitive **alb**-net. Atom color scheme: C, gray; Zr, bright green; O, red. H atoms have been omitted for the sake of clarity.

performance toward the destruction of nerve agent simulants in the presence of both liquid and solid bases.

The **alb** net, constructed from 6-c trigonal-prismatic SBUs and 12-c hexagonal-prismatic SBUs, is one of the most intriguing binodal edge-transitive nets.[21] The (6,12)-c **alb** net is a highly connected net that could potentially be realized in Zr-MOFs by rational design and precise control of the geometry of the organic linkers. In this work, the augmented **alb** (**alb**-a) net was used to illustrate the topological network. Threefold-disordered Zr_6 nodes have been observed in PCN-223[42] and NU-904[44] with the overall topology of the 4,12-c **shp** net, where the Zr_6 nodes can be viewed as rare hexagonal-prismatic SBUs. We anticipated that the use of rigid trigonal-prismatic PET-1 ligands would guide the in situ formation of 12-c Zr_6 nodes as hexagonal-prismatic SBUs, thus resulting in a 3-periodic structure with the **alb** net.

Indeed, single crystals of NU-1600 (Figure 2) with suitable sizes for SCXRD investigation were obtained after careful fine-tuning of the synthetic conditions—i.e., $ZrCl_4$, PET-1, and acidic modulators were dissolved in *N*,*N*-diethylformamide (DEF), and the mixture was then kept at 130 °C for 4 days. SCXRD analysis revealed that NU-1600 crystallizes in space group $P2/m$ (a = 21.632(1) Å, b = 12.2815(5) Å, c = 21.627 (1) Å, and β = 119.975(2)° at 100 K) with an ideal formula $Zr_6(\mu_3\text{-}O)_2(\mu_3\text{-}OH)_6(HCOO)(OH)(H_2O)(PET\text{-}1)_2$, without considering the missing-linker defects (Table S1 and Figure S2). Each PET-1 ligand of NU-1600 is coordinated to six Zr_6 nodes, and each threefold-disordered Zr_6 node is coordinated to 12 PET-1 linkers, rendering the expected 6,12-c **alb** net. The 12-c Zr_6 node of NU-1600, which can be viewed as a hexagonal-prismatic SBU, is different from the 12-c Zr_6 node of UiO-66—i.e., a cuboctahedron SBU (Figure S3). To the best of our knowledge, the **alb** net was a missing edge-transitive net for the well-

DOI: 10.1021/jacs.9b06179
J. Am. Chem. Soc. XXXX, XXX, XXX−XXX

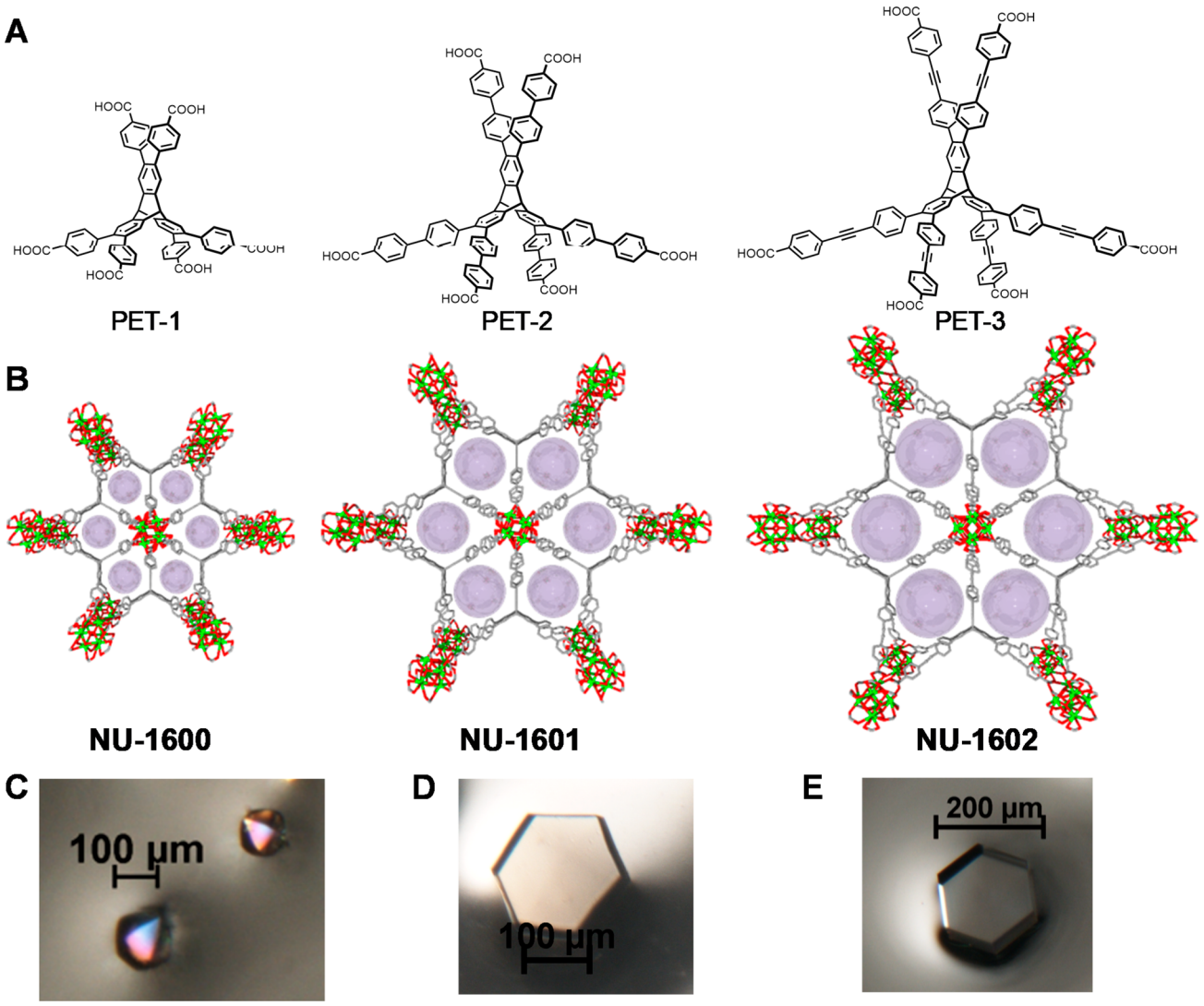

Figure 2. (A) Structures of organic ligands used in this work. (B) Representative structures of NU-1600, NU-1601, and NU-1602 viewed along the *b* axis. (C−E) Optical images of single crystals of (C) NU-1600, (D) NU-1601, and (E) NU-1602.

developed functional Zr-MOFs until we uncovered it. NU-1600 can alternatively be further analyzed as an (3,3,12)-c **alb**-*derived* **ury** net if the ligand is deconstructed into two 3-c SBUs.[24,43]

NU-1600 contains one type of diamond-shaped channels with a dimension of ca. 1.1 nm along the *b* axis and two-dimensional honeycomb-shaped channels in the *ac* plane (Figure S4). The microcrystalline sample of NU-1600 was synthesized with sizes of 1−2 μm, as revealed by scanning electron microscopy (SEM) (Figure S11). The phase purity of the bulk NU-1600 was confirmed by the well-matched simulated and as-synthesized powder X-ray diffraction (PXRD) patterns (Figure S5). The permanent porosity of NU-1600 was confirmed by the N_2 adsorption isotherm at 77 K with an estimated apparent BET surface area of 2085 $m^2\ g^{-1}$ (Figures 3 and S14). It is interesting to note that the experimental total PV of 0.82 $cm^3\ g^{-1}$ is higher than the simulated value—i.e., 0.69 $cm^3\ g^{-1}$—for the structure when PET-1 has 100% occupancy inside NU-1600 but agrees well with the simulated PV—i.e., 0.83 $cm^3\ g^{-1}$—when PET-1 has 70% occupancy (Table S5). In fact, the best crystallographic refinement of the SCXRD data was obtained for NU-1600 when the occupancy level of PET-1 is around 70%, indicating the presence of missing-linker defects.[46−48] The pore size distribution based on a density functional theory (DFT) model from the N_2 adsorption isotherm revealed one type of main pore centered at 1.2 nm (Figure 3B), which agrees with the size of the diamond-shaped channels. Extra pores ranging from 1.5 to 2.2 nm could be associated with the missing-linker defects.

Highly connected edge-transitive nets induce higher degrees of designability with precise choices of building units. They offer more possibilities toward elongated isoreticular structures without catenation.[24,26,49−51] Solvothermal reactions of longer peripherally extended triptycene ligands—i.e., H_6PET-2 and H_6PET-3—and $ZrCl_4$ under synthetic conditions similar to those for NU-1600 yielded colorless hexagonal block crystals of NU-1601 and NU-1602, respectively. SCXRD studies revealed that both materials have noncatenated structures crystallizing in space group *P*2/*m* (NU-1601: a = 28.130(3), b = 16.735(2), c = 28.174(3) (1) Å, and β = 120.036(4)° at 275 K; NU-1602: a = 31.678(8), b = 19.591(4), c = 31.774(1) Å, and β = 119.631(2)° at 275 K). The phase purities of bulk NU-1601 and NU-1602 were confirmed by the well-matched simulated and as-synthesized PXRD patterns (Figures S6 and S7). Topological analysis revealed that NU-1601 and NU-1602 have the same underlying 6,12-c **alb** topology as NU-1600 with threefold-

DOI: 10.1021/jacs.9b06179
J. Am. Chem. Soc. XXXX, XXX, XXX−XXX

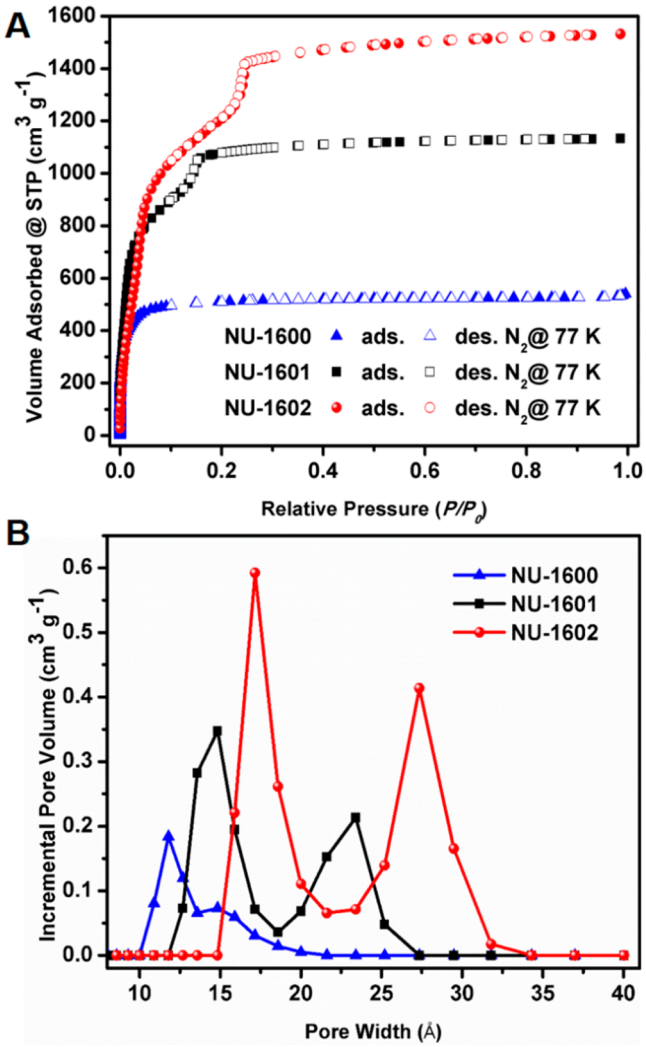

Figure 3. (A) Experimental N_2 adsorption and desorption isotherms at 77 K and (B) DFT pore size distributions for NU-1600, NU-1601, and NU-1602.

disordered Zr_6 nodes and extended PET ligands as 12-c hexagonal-prismatic and 6-c trigonal-prismatic SBUs, respectively.

N_2 adsorption isotherms of NU-1601 and NU-1602 at 77 K after supercritical CO_2 activation revealed that both structures are mesoporous MOFs with experimental total PVs of 1.75 and 2.36 $cm^3\ g^{-1}$, respectively, at $P/P_0 = 0.95$. NU-1601 and NU-1602 exhibited N_2 uptakes of 1133 and 1531 $cm^3\ g^{-1}$, respectively at 77 K and $P/P_0 = 0.95$. The pore size distributions of NU-1601 and NU-1602 based on DFT models from the N_2 adsorption isotherms revealed main pores centered at 1.4 and 1.7 nm, respectively, which agree with the sizes of the diamond channels. Similar to NU-1600, the extra mesopores—i.e., 2.2 and 2.7 nm—can be attributed to missing-linker defects. The apparent BET areas of NU-1601 and NU-1602 were estimated to be 3970 and 4500 $m^2\ g^{-1}$, respectively, after the four BET consistency criteria were satisfied with correlation coefficients higher than 0.995 (Figures S15 and S16 and Table S4).[52]

Zr-MOFs have been widely evaluated for the hydrolysis of dimethyl 4-nitrophenyl phosphonate (DMNP), a nerve agent simulant mimicking the reactivity of organophosphonate-based nerve agents, on account of Lewis acidic sites on the Zr_6 nodes.[4,53−58] However, systematic studies of isoreticular

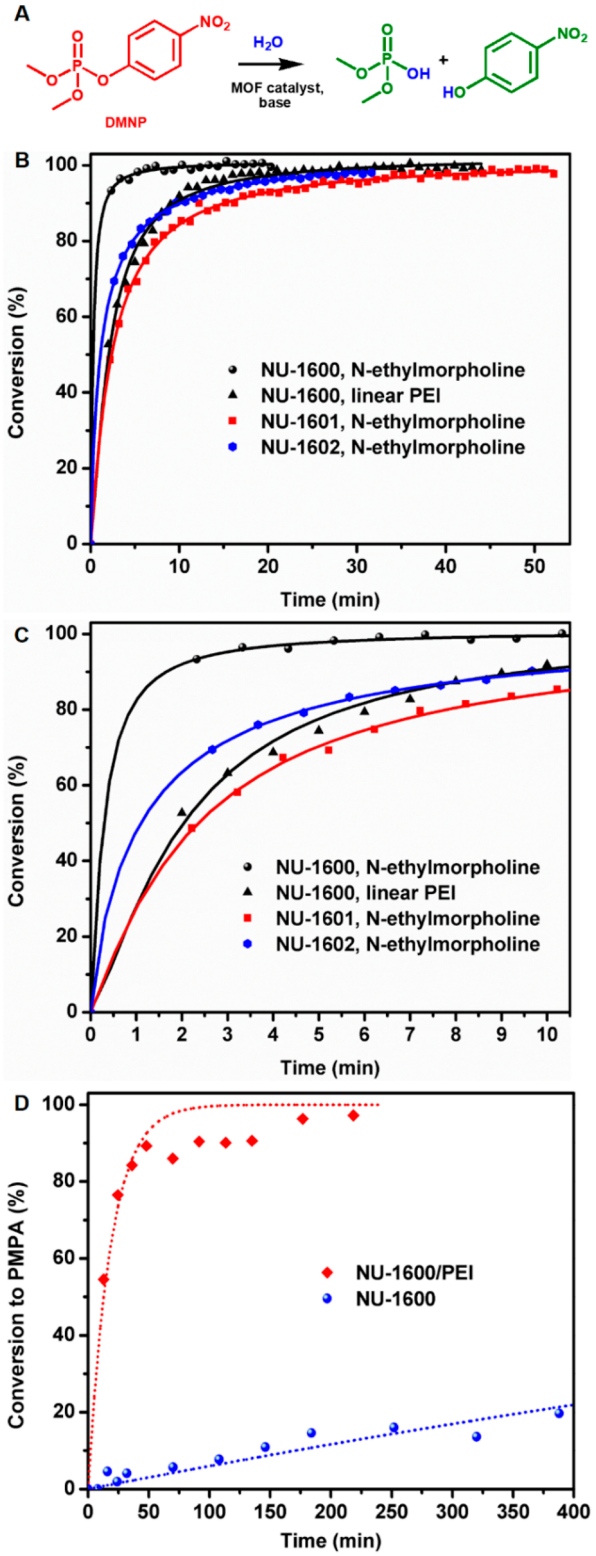

Figure 4. (A) Hydrolysis reaction of DMNP. (B) Hydrolysis profiles of DMNP with NU-160*X* (*X* = 0, 1, 2) using 6 mol % catalyst loadings in the presence of different bases: *N*-ethylmorpholine and linear PEI. (C) First 10 min of the hydrolysis profile shown in (B) for clarity. Solid lines are used as guides. (D) Conversion vs time data for NU-1600 and NU-1600/PEI for the hydrolysis of soman. Dotted lines correspond to first-order fits.

MOFs with similar Zr_6 nodes and pore sizes ranging from micropore to mesopore are still limited. Herein, taking

DOI: 10.1021/jacs.9b06179
J. Am. Chem. Soc. XXXX, XXX, XXX−XXX

advantage of the missing-linker defects in NU-160*X* (*X* = 0, 1, 2), which expose the Lewis acidic sites on the Zr nodes, we explored the hydrolysis of DMNP using microsized (1−4 μm) crystals of NU-160*X* (*X* = 0, 1, 2) (Figures S11−S13) in the presence of liquid *N*-ethylmorpholine and solid linear polyethylenimine (PEI) (Figures 4, S17, and S18). The initial half-life of DMNP in the presence of *N*-ethylmorpholine with NU-1600 (6 mol % catalyst loading) was quite short ($t_{1/2} \approx 1$ min), with a turnover frequency (TOF) of 0.21 s^{-1}. Under the same conditions, the hydrolysis of DMNP exhibited similar TOFs, namely, 0.22 and 0.15 s^{-1} for catalyst loadings of 3 and 1.5 mol %, respectively (Tables S6 and S7).

Moreover, NU-1600 can efficiently hydrolyze DMNP in the presence of a solid base—i.e., linear PEI—with $t_{1/2} \approx 3$ min and TOF = 0.05 s^{-1}. After washing with water, the NU-1600/PEI composite displays similar reactivity, confirming the heterogeneous nature of the PEI base (Figure S19), which is more practical for protective suit and mask applications.[54] NU-1601 and NU-1602 show similar performance as NU-1600 toward the hydrolysis of DMNP, but the hydrolysis is slightly slower ($t_{1/2} \approx$ 3.2 and 2.5 min, respectively). These data suggest that the higher degree of missing-linker defects in NU-1600 compared with either NU-1601 or NU-1602, as illustrated by thermogravimetric analysis (TGA) under air flow (Figures S8−S10 and Table S3), induces a larger number of Lewis acidic Zr catalytic sites for the hydrolysis to occur, since the particle sizes of these isostructural materials are similar.

The NU-1600/PEI composite enhances the hydrolysis rate of an actual nerve agent, soman (GD), compared with NU-1600. The conversion of GD to the nontoxic pinacolyl methylphosphonic acid (PMPA) as a function of time is shown in Figure 4D, and ^{31}P NMR spectra show the conversion of PMPA (Figures S20−S22). The enhanced reactivity arising from the solid-phase PEI base is clear, with 50% of GD reacting in the presence of NU-1600/PEI sample in under 12 min, compared with only 20% of GD reacting on baseline NU-1600 after 400 min. The rate constants calculated from a first-order kinetic model are 6.2 $\times 10^{-4}$ and 5.4 $\times 10^{-2}$ min^{-1} for NU-1600 and NU-1600/PEI, respectively. These results demonstrated that the NU-1600/PEI composite can efficiently detoxify the chemical warfare agent.

In conclusion, we have rationally designed and synthesized a series of missing Zr-MOFs, the NU-160*X* series (*X* = 0, 1, 2), with the *edge-transitive* 6,12-c **alb** topology. The highly connected **alb** net provides a blueprint for programmable noncatenated MOF structures with tunable surface areas and tailorable porosities ranging from microporous to mesoporous. These structurally defective Zr-MOFs display notable activities toward the efficient destruction of a nerve agent as well as its simulant in the presence of liquid and solid bases. This research illustrates the power of reticular chemistry for the rational design and synthesis of functional highly connected materials and paves the way for correlating unique material properties with desired functionalities.

■ ASSOCIATED CONTENT

Supporting Information

The Supporting Information is available free of charge on the ACS Publications website at DOI: 10.1021/jacs.9b06179.

Synthetic procedures for MOF materials, comparison of Zr-MOFs with edge-transitive nets, crystallographic data, PXRD patterns, SEM data, additional low-pressure sorption isotherms, and BET area calculations (PDF)

Crystallographic data for NU-1600 (CIF)

Crystallographic data for NU-1601 (CIF)

Crystallographic data for NU-1602 (CIF)

■ AUTHOR INFORMATION

Corresponding Author

*o-farha@northwestern.edu

ORCID

Zhijie Chen: 0000-0001-9232-7382
Penghao Li: 0000-0002-1517-5845
Xingjie Wang: 0000-0002-5802-9944
Ken-ichi Otake: 0000-0002-7904-5003
Xuan Zhang: 0000-0001-8214-7265
Lee Robison: 0000-0002-7419-4499
Timur Islamoglu: 0000-0003-3688-9158
Gregory W. Peterson: 0000-0003-3467-5295
J. Fraser Stoddart: 0000-0003-3161-3697
Omar K. Farha: 0000-0002-9904-9845

Notes

The authors declare no competing financial interest.

■ ACKNOWLEDGMENTS

O.K.F. gratefully acknowledges support from the Defense Threat Reduction Agency (HDTRA1-18-1-0003 for catalysis and HDTRA1-19-1-0007 for MOF synthesis). This work made use of the EPIC facility of Northwestern University's NUANCE Center, which has received support from the Soft and Hybrid Nanotechnology Experimental (SHyNE) Resource (NSF NNCI-1542205); the MRSEC program (NSF DMR-1720139) at the Materials Research Center; the International Institute for Nanotechnology (IIN); the Keck Foundation; and the State of Illinois through the IIN. This work made use of the IMSERC at Northwestern University, which has received support from the NSF (CHE-1048773 and DMR0521267); the SHyNE Resource (NSF NNCI-1542205); the State of Illinois, and the IIN. P.L. and J.F.S. acknowledge the Joint Center of Excellence in Integrated Nano-Systems (JCIN) at King Abdulaziz City for Science and Technology (KACST) and Northwestern University (NU). G.W.P. and M.H. gratefully acknowledge support from the Defense Threat Reduction Agency under Grant CB3934 for the hydrolysis of GD. We thanks Margaret E. Schott for the proofreading of this paper.

■ REFERENCES

(1) Furukawa, H.; Cordova, K. E.; O'Keeffe, M.; Yaghi, O. M. The chemistry and applications of metal-organic frameworks. *Science* **2013**, *341*, 1230444.

(2) Kitagawa, S.; Kitaura, R.; Noro, S. Functional porous coordination polymers. *Angew. Chem., Int. Ed.* **2004**, *43*, 2334−2375.

(3) Cavka, J. H.; Jakobsen, S.; Olsbye, U.; Guillou, N.; Lamberti, C.; Bordiga, S.; Lillerud, K. P. A new zirconium inorganic building brick forming metal organic frameworks with exceptional stability. *J. Am. Chem. Soc.* **2008**, *130*, 13850−13851.

(4) Mondloch, J. E.; Katz, M. J.; Isley, W. C., Iii; Ghosh, P.; Liao, P.; Bury, W.; Wagner, G. W.; Hall, M. G.; DeCoste, J. B.; Peterson, G. W.; Snurr, R. Q.; Cramer, C. J.; Hupp, J. T.; Farha, O. K. Destruction of chemical warfare agents using metal−organic frameworks. *Nat. Mater.* **2015**, *14*, 512−516.

(5) Liu, Y.; Xuan, W.; Cui, Y. Engineering homochiral metal-organic frameworks for heterogeneous asymmetric catalysis and enantioselective separation. *Adv. Mater.* **2010**, *22*, 4112−4135.

DOI: 10.1021/jacs.9b06179
J. Am. Chem. Soc. XXXX, XXX, XXX−XXX

(6) Zhang, T.; Lin, W. Metal-organic frameworks for artificial photosynthesis and photocatalysis. *Chem. Soc. Rev.* **2014**, *43*, 5982−5993.
(7) Liu, J.; Chen, L.; Cui, H.; Zhang, J.; Zhang, L.; Su, C.-Y. Applications of metal-organic frameworks in heterogeneous supramolecular catalysis. *Chem. Soc. Rev.* **2014**, *43*, 6011−6061.
(8) Zhang, X.; Huang, Z.; Ferrandon, M.; Yang, D.; Robison, L.; Li, P.; Wang, T. C.; Delferro, M.; Farha, O. K. Catalytic chemoselective functionalization of methane in a metal−organic framework. *Nat. Catal.* **2018**, *1*, 356−362.
(9) Rogge, S. M. J.; Bavykina, A.; Hajek, J.; Garcia, H.; Olivos-Suarez, A. I.; Sepúlveda-Escribano, A.; Vimont, A.; Clet, G.; Bazin, P.; Kapteijn, F.; Daturi, M.; Ramos-Fernandez, E. V.; Llabrés i Xamena, F. X.; Van Speybroeck, V.; Gascon, J. Metal−organic and covalent organic frameworks as single-site catalysts. *Chem. Soc. Rev.* **2017**, *46*, 3134−3184.
(10) Hu, Z.; Deibert, B. J.; Li, J. Luminescent metal-organic frameworks for chemical sensing and explosive detection. *Chem. Soc. Rev.* **2014**, *43*, 5815−5840.
(11) Cui, Y.; Yue, Y.; Qian, G.; Chen, B. Luminescent functional metal−organic frameworks. *Chem. Rev.* **2012**, *112*, 1126−1162.
(12) Dolgopolova, E. A.; Rice, A. M.; Martin, C. R.; Shustova, N. B. Photochemistry and photophysics of MOFs: Steps towards MOF-based sensing enhancements. *Chem. Soc. Rev.* **2018**, *47*, 4710−4728.
(13) Drout, R. J.; Robison, L.; Chen, Z.; Islamoglu, T.; Farha, O. K. Zirconium metal−organic frameworks for organic pollutant adsorption. *Trends Chem.* **2019**, *1*, 304−317.
(14) Mon, M.; Bruno, R.; Ferrando-Soria, J.; Armentano, D.; Pardo, E. Metal−organic framework technologies for water remediation: Towards a sustainable ecosystem. *J. Mater. Chem. A* **2018**, *6*, 4912−4947.
(15) Mason, J. A.; Oktawiec, J.; Taylor, M. K.; Hudson, M. R.; Rodriguez, J.; Bachman, J. E.; Gonzalez, M. I.; Cervellino, A.; Guagliardi, A.; Brown, C. M.; Llewellyn, P. L.; Masciocchi, N.; Long, J. R. Methane storage in flexible metal−organic frameworks with intrinsic thermal management. *Nature* **2015**, *527*, 357−361.
(16) Cadiau, A.; Adil, K.; Bhatt, P. M.; Belmabkhout, Y.; Eddaoudi, M. A metal-organic framework−based splitter for separating propylene from propane. *Science* **2016**, *353*, 137−140.
(17) Cui, X.; Chen, K.; Xing, H.; Yang, Q.; Krishna, R.; Bao, Z.; Wu, H.; Zhou, W.; Dong, X.; Han, Y.; Li, B.; Ren, Q.; Zaworotko, M. J.; Chen, B. Pore chemistry and size control in hybrid porous materials for acetylene capture from ethylene. *Science* **2016**, *353*, 141−144.
(18) Liao, P.-Q.; Huang, N.-Y.; Zhang, W.-X.; Zhang, J.-P.; Chen, X.-M. Controlling guest conformation for efficient purification of butadiene. *Science* **2017**, *356*, 1193−1196.
(19) Banerjee, D.; Cairns, A. J.; Liu, J.; Motkuri, R. K.; Nune, S. K.; Fernandez, C. A.; Krishna, R.; Strachan, D. M.; Thallapally, P. K. Potential of metal−organic frameworks for separation of xenon and krypton. *Acc. Chem. Res.* **2015**, *48*, 211−219.
(20) Yaghi, O. M.; O'Keeffe, M.; Ockwig, N. W.; Chae, H. K.; Eddaoudi, M.; Kim, J. Reticular synthesis and the design of new materials. *Nature* **2003**, *423*, 705−714.
(21) Delgado-Friedrichs, O.; O'Keeffe, M.; Yaghi, O. M. Three-periodic nets and tilings: Edge-transitive binodal structures. *Acta Crystallogr., Sect. A: Found. Crystallogr.* **2006**, *62*, 350−355.
(22) Zhang, M.; Chen, Y.-P.; Bosch, M.; Gentle, T.; Wang, K.; Feng, D.; Wang, Z. U.; Zhou, H.-C. Symmetry-guided synthesis of highly porous metal−organic frameworks with fluorite topology. *Angew. Chem., Int. Ed.* **2014**, *53*, 815−818.
(23) Yaghi, O. M. Reticular chemistry—Construction, properties, and precision reactions of frameworks. *J. Am. Chem. Soc.* **2016**, *138*, 15507−15509.
(24) Chen, Z.; Weseliński, Ł. J.; Adil, K.; Belmabkhout, Y.; Shkurenko, A.; Jiang, H.; Bhatt, P. M.; Guillerm, V.; Dauzon, E.; Xue, D.-X.; O'Keeffe, M.; Eddaoudi, M. Applying the power of reticular chemistry to finding the missing **alb**-MOF platform based on the (6,12)-coordinated edge-transitive net. *J. Am. Chem. Soc.* **2017**, *139*, 3265−3274.
(25) Chen, Z.; Li, P.; Zhang, X.; Li, P.; Wasson, M. C.; Islamoglu, T.; Stoddart, J. F.; Farha, O. K. Reticular access to highly porous **acs**-MOFs with rigid trigonal prismatic linkers for water sorption. *J. Am. Chem. Soc.* **2019**, *141*, 2900−2905.
(26) Guillerm, V.; Weseliński, Ł. J.; Belmabkhout, Y.; Cairns, A. J.; D'Elia, V.; Wojtas, Ł.; Adil, K.; Eddaoudi, M. Discovery and introduction of a (3,18)-connected net as an ideal blueprint for the design of metal−organic frameworks. *Nat. Chem.* **2014**, *6*, 673−680.
(27) Ramaswamy, P.; Wong, N. E.; Shimizu, G. K. H. MOFs as proton conductors − Challenges and opportunities. *Chem. Soc. Rev.* **2014**, *43*, 5913−5932.
(28) Chen, Z.; Hanna, S. L.; Redfern, L. R.; Alezi, D.; Islamoglu, T.; Farha, O. K. Reticular chemistry in the rational synthesis of functional zirconium cluster-based MOFs. *Coord. Chem. Rev.* **2019**, *386*, 32−49.
(29) Kalidindi, S. B.; Nayak, S.; Briggs, M. E.; Jansat, S.; Katsoulidis, A. P.; Miller, G. J.; Warren, J. E.; Antypov, D.; Corà, F.; Slater, B.; Prestly, M. R.; Martí-Gastaldo, C.; Rosseinsky, M. J. Chemical and structural stability of zirconium-based metal−organic frameworks with large three-dimensional pores by linker engineering. *Angew. Chem., Int. Ed.* **2015**, *54*, 221−226.
(30) Bai, Y.; Dou, Y.; Xie, L.-H.; Rutledge, W.; Li, J.-R.; Zhou, H.-C. Zr-based metal-organic frameworks: Design, synthesis, structure, and applications. *Chem. Soc. Rev.* **2016**, *45*, 2327−2367.
(31) Furukawa, H.; Gándara, F.; Zhang, Y.-B.; Jiang, J.; Queen, W. L.; Hudson, M. R.; Yaghi, O. M. Water adsorption in porous metal−organic frameworks and related materials. *J. Am. Chem. Soc.* **2014**, *136*, 4369−4381.
(32) Wang, S.; Lee, J. S.; Wahiduzzaman, M.; Park, J.; Muschi, M.; Martineau-Corcos, C.; Tissot, A.; Cho, K. H.; Marrot, J.; Shepard, W.; Maurin, G.; Chang, J.-S.; Serre, C. A robust large-pore zirconium carboxylate metal−organic framework for energy-efficient water-sorption-driven refrigeration. *Nat. Energy* **2018**, *3*, 985−993.
(33) Feng, D.; Chung, W.-C.; Wei, Z.; Gu, Z.-Y.; Jiang, H.-L.; Chen, Y.-P.; Darensbourg, D. J.; Zhou, H.-C. Construction of ultrastable porphyrin Zr metal−organic frameworks through linker elimination. *J. Am. Chem. Soc.* **2013**, *135*, 17105−17110.
(34) Alezi, D.; Spanopoulos, I.; Tsangarakis, C.; Shkurenko, A.; Adil, K.; Belmabkhout, Y.; O'Keeffe, M.; Eddaoudi, M.; Trikalitis, P. N. Reticular chemistry at its best: Directed assembly of hexagonal building units into the awaited metal-organic framework with the intricate polybenzene topology, **pbz**-MOF. *J. Am. Chem. Soc.* **2016**, *138*, 12767−12770.
(35) Liu, T.-F.; Vermeulen, N. A.; Howarth, A. J.; Li, P.; Sarjeant, A. A.; Hupp, J. T.; Farha, O. K. Adding to the arsenal of zirconium-based metal−organic frameworks: The topology as a platform for solvent-assisted metal incorporation. *Eur. J. Inorg. Chem.* **2016**, *2016*, 4349−4352.
(36) Wang, B.; Lv, X.-L.; Feng, D.; Xie, L.-H.; Zhang, J.; Li, M.; Xie, Y.; Li, J.-R.; Zhou, H.-C. Highly stable Zr(IV)-based metal−organic frameworks for the detection and removal of antibiotics and organic explosives in water. *J. Am. Chem. Soc.* **2016**, *138*, 6204−6216.
(37) Feng, D.; Gu, Z.-Y.; Li, J.-R.; Jiang, H.-L.; Wei, Z.; Zhou, H.-C. Zirconium-metalloporphyrin PCN-222: Mesoporous metal−organic frameworks with ultrahigh stability as biomimetic catalysts. *Angew. Chem., Int. Ed.* **2012**, *51*, 10307−10310.
(38) Morris, W.; Volosskiy, B.; Demir, S.; Gándara, F.; McGrier, P. L.; Furukawa, H.; Cascio, D.; Stoddart, J. F.; Yaghi, O. M. Synthesis, structure, and metalation of two new highly porous zirconium metal−organic frameworks. *Inorg. Chem.* **2012**, *51*, 6443−6445.
(39) Mondloch, J. E.; Bury, W.; Fairen-Jimenez, D.; Kwon, S.; DeMarco, E. J.; Weston, M. H.; Sarjeant, A. A.; Nguyen, S. T.; Stair, P. C.; Snurr, R. Q.; Farha, O. K.; Hupp, J. T. Vapor-phase metalation by atomic layer deposition in a metal−organic framework. *J. Am. Chem. Soc.* **2013**, *135*, 10294−10297.
(40) Bon, V.; Senkovskyy, V.; Senkovska, I.; Kaskel, S. Zr(IV) and Hf(IV) based metal-organic frameworks with reo-topology. *Chem. Commun.* **2012**, *48*, 8407−8409.
(41) Muldoon, P. F.; Liu, C.; Miller, C. C.; Koby, S. B.; Gamble Jarvi, A.; Luo, T.-Y.; Saxena, S.; O'Keeffe, M.; Rosi, N. L. Programmable

DOI: 10.1021/jacs.9b06179
J. Am. Chem. Soc. XXXX, XXX, XXX−XXX

topology in new families of heterobimetallic metal−organic frameworks. *J. Am. Chem. Soc.* **2018**, *140*, 6194−6198.
(42) Feng, D.; Gu, Z.-Y.; Chen, Y.-P.; Park, J.; Wei, Z.; Sun, Y.; Bosch, M.; Yuan, S.; Zhou, H.-C. A highly stable porphyrinic zirconium metal−organic framework with **shp-a** topology. *J. Am. Chem. Soc.* **2014**, *136*, 17714−17717.
(43) Chen, Z.; Jiang, H.; O'Keeffe, M.; Eddaoudi, M. Minimal edge-transitive nets for the design and construction of metal-organic frameworks. *Faraday Discuss.* **2017**, *201*, 127−143.
(44) Lyu, J.; Zhang, X.; Otake, K.-i.; Wang, X.; Li, P.; Li, Z.; Chen, Z.; Zhang, Y.; Wasson, M. C.; Yang, Y.; Bai, P.; Guo, X.; Islamoglu, T.; Farha, O. K. Topology and porosity control of metal−organic frameworks through linker functionalization. *Chem. Sci.* **2019**, *10*, 1186−1192.
(45) Li, P.; Li, P.; Ryder, M. R.; Liu, Z.; Stern, C. L.; Farha, O. K.; Stoddart, J. F. Interpenetration isomerism in triptycene-based hydrogen-bonded organic frameworks. *Angew. Chem., Int. Ed.* **2019**, *58*, 1664−1669.
(46) Valenzano, L.; Civalleri, B.; Chavan, S.; Bordiga, S.; Nilsen, M. H.; Jakobsen, S.; Lillerud, K. P.; Lamberti, C. Disclosing the complex structure of UiO-66 metal organic framework: A synergic combination of experiment and theory. *Chem. Mater.* **2011**, *23*, 1700−1718.
(47) Wu, H.; Chua, Y. S.; Krungleviciute, V.; Tyagi, M.; Chen, P.; Yildirim, T.; Zhou, W. Unusual and highly tunable missing-linker defects in zirconium metal−organic framework UiO-66 and their important effects on gas adsorption. *J. Am. Chem. Soc.* **2013**, *135*, 10525−10532.
(48) Liu, L.; Chen, Z.; Wang, J.; Zhang, D.; Zhu, Y.; Ling, S.; Huang, K.-W.; Belmabkhout, Y.; Adil, K.; Zhang, Y.; Slater, B.; Eddaoudi, M.; Han, Y. Imaging defects and their evolution in a metal−organic framework at sub-unit-cell resolution. *Nat. Chem.* **2019**, *11*, 622−628.
(49) Liu, T.-F.; Feng, D.; Chen, Y.-P.; Zou, L.; Bosch, M.; Yuan, S.; Wei, Z.; Fordham, S.; Wang, K.; Zhou, H.-C. Topology-guided design and syntheses of highly stable mesoporous porphyrinic zirconium metal−organic frameworks with high surface area. *J. Am. Chem. Soc.* **2015**, *137*, 413−419.
(50) Lin, Q.; Bu, X.; Kong, A.; Mao, C.; Zhao, X.; Bu, F.; Feng, P. New heterometallic zirconium metalloporphyrin frameworks and their heteroatom-activated high-surface-area carbon derivatives. *J. Am. Chem. Soc.* **2015**, *137*, 2235−2238.
(51) Zheng, J.; Wu, M.; Jiang, F.; Su, W.; Hong, M. Stable porphyrin Zr and Hf metal−organic frameworks featuring 2.5 nm cages: High surface areas, scsc transformations and catalyses. *Chem. Sci.* **2015**, *6*, 3466−3470.
(52) Gómez-Gualdrón, D. A.; Moghadam, P. Z.; Hupp, J. T.; Farha, O. K.; Snurr, R. Q. Application of consistency criteria to calculate BET areas of micro- and mesoporous metal−organic frameworks. *J. Am. Chem. Soc.* **2016**, *138*, 215−224.
(53) DeCoste, J. B.; Peterson, G. W. Metal−organic frameworks for air purification of toxic chemicals. *Chem. Rev.* **2014**, *114*, 5695−5727.
(54) Chen, Z.; Islamoglu, T.; Farha, O. K. Toward base heterogenization: A zirconium metal−organic framework/dendrimer or polymer mixture for rapid hydrolysis of a nerve-agent simulant. *ACS Appl. Nano Mater.* **2019**, *2*, 1005−1008.
(55) Palomba, J. M.; Credille, C. V.; Kalaj, M.; DeCoste, J. B.; Peterson, G. W.; Tovar, T. M.; Cohen, S. M. High-throughput screening of solid-state catalysts for nerve agent degradation. *Chem. Commun.* **2018**, *54*, 5768−5771.
(56) Gil-San-Millan, R.; López-Maya, E.; Hall, M.; Padial, N. M.; Peterson, G. W.; DeCoste, J. B.; Rodríguez-Albelo, L. M.; Oltra, J. E.; Barea, E.; Navarro, J. A. R. Chemical warfare agents detoxification properties of zirconium metal−organic frameworks by synergistic incorporation of nucleophilic and basic sites. *ACS Appl. Mater. Interfaces* **2017**, *9*, 23967−23973.
(57) Ryu, S. G.; Kim, M.-K.; Park, M.; Jang, S. O.; Kim, S. H.; Jung, H. Availability of Zr-based MOFs for the degradation of nerve agents in all humidity conditions. *Microporous Mesoporous Mater.* **2019**, *274*, 9−16.
(58) de Koning, M. C.; van Grol, M.; Breijaert, T. Degradation of paraoxon and the chemical warfare agents VX, tabun, and soman by the metal−organic frameworks UiO-66-NH_2, MOF-808, NU-1000, and PCN-777. *Inorg. Chem.* **2017**, *56*, 11804−11809.

DOI: 10.1021/jacs.9b06179
J. Am. Chem. Soc. XXXX, XXX, XXX−XXX